Conf. Paper number 3107-08 ~~3105~~

1418

A Very Efficient Sampling Technique for Fibre-Remote Optical Emission Spectroscopy of Aqueous Solutions

Steven J. Mackenzie[a], Jane Hodgkinson[b], Mark Johnson[b], and John P. Dakin[c]
[a]The Optoelectronics Research Centre, Southampton University, UK, SO17 1BJ
[b]North West Water Ltd, Dawson House, Warrington, UK, WA5 3LW
[c]Department of Electronics and Computer Science, Southampton University, UK, SO17 1BJ

ABSTRACT

We have measured fluorescence from a waveguide formed by a falling cylindrical stream of liquid. The configuration is suited to taking measurements from liquids with any refractive index, such as aqueous solutions. The parameters which determine the stream stability have been investigated, and the optical collection efficiency has been mathematically modelled. We have produced streams up to 350 mm long with a 2.5 mm diameter, and measured a fluorescence collection enhancement factor of 9 from a 100 mm long, 1 mm diameter stream.

Keywords: water, aqueous, fluorescence, Raman, optical fiber, spectroscopy, falling analyte stream

1. INTRODUCTION

Measurements of optical emission, such as Raman scattered light or fluorescence, are widely used in chemical analysis. However, measurements of low intensity emission require that maximum use is made of all the available light.

In order to increase the total amount of light collected in emission spectroscopies, optical fibre probes have been coupled with capillary type cells. If the refractive index of the capillary is greater than that of the analyte, then a waveguide is formed, and light will be tightly confined within the analyte. If the capillary diameter matches the probe diameter, then scattered light is efficiently coupled into the probe. By using very long capillaries this arrangement can increase the signal collected by several orders of magnitude[1].

Unfortunately this has not previously been possible for most aqueous solutions, because the refractive index of water, n=1.33, is lower than that of most suitable cell materials (for instance, silica glass has n=1.47, and poly [tetrafluoroethlylene] (PTFE)[2] has n=1.34). We have proposed two cell designs which are compatible with the analysis of aqueous solutions.

The first method, which has already been presented at this conference in the chemical sensing session[3], is to use a low-refractive-index polymer-capillary tube. The Du Pont material Teflon AF-1600 is a copolymer of PTFE and poly [2,2-bistrifluoromethyl-4,5-difluoro-1,3-dioxole] (PDD), with a refractive index of 1.32, and so it is suitable for forming low index capillary tubes. Unfortunately it is very expensive (~US$40/g), and requires specialised processing to fabricate tubes. We have overcome these problems by depositing a film up to 10 micron thick on to the inside of a commercial PTFE tube.

In the second method, presented here, the cladding of the waveguide has been dispensed with altogether and the analyte alone forms a very efficient waveguide (see figure 1). By shaping the analyte into a cylinder surrounded by air, light is reflected at the boundary between the analyte and air by total internal reflection. An aqueous solution of a fluorescent dye was circulated around a flow rig, which produced stable falling analyte streams through nozzles of internal diameter 1.0, 1.5, 2.0, and 2.5 mm. Excitation light was coupled into the base of the stream with a multiple optical fibre probe. A proportion of the light emitted within the stream was collected from the base of the stream using the same probe, and transmitted to a CCD spectrograph.

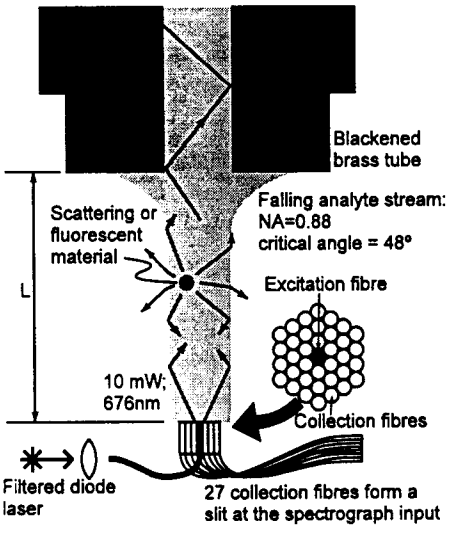

Figure 1 Efficient collection of emitted light, using a falling analyte stream which is coupled to an optical fibre bundle. The complete system is shown in figure 8.

2. THEORY

Mechanical factors affecting the stream are described, and applied to the production of streams of optimum shape. We also consider how the numerical aperture of the cylinder and the sample absorbance affect the signal enhancement.

2.1. Stream mechanics

The stability of water streams was considered by Rayleigh[4], who found that low frequency vibrations originating at the jet orifice would tend to grow exponentially as the water falls. (Here, *low frequency* is taken to mean vibrations with a wavelength in water larger than the orifice diameter; for a diameter of 1mm, this limits the discussion to acoustic vibrations with frequencies below 1.5MHz.) Rayleigh noted, "Even though no regular vibration has access to the nozzle, the instability cannot fail to assert itself, and causal disturbances of a complex character will bring about disintegration." Thus, the stable length of the water stream can be extended, by isolating the stream acoustically from its environment, but stream instabilities cannot be eliminated.

The effect of externally-applied audio-frequency disturbances to water streams has been examined[5], and we have incorporated some of the suggestions of that study in this work. To reduce the effect of background noise flexible tubing was incorporated to isolate the apparatus, and a buffer chamber was used above the stream to reduce turbulence in the fluid.

2.1.1. Stream stability

A more recent treatment of low velocity liquid streams has been given by Weber[6]. His formula for the critical length of a water stream (the stable length of the stream) is given in equation 1.

$$z_c = \frac{2vR_c}{\gamma}\left(\sqrt{2\rho\gamma R_c} + 3\eta\right)\log_e\left(\frac{R_c}{\psi}\right) \qquad (1)$$

Here z_c is the critical (stable) length of the stream, R_c is the critical radius of the stream, v is the average fluid velocity at the break-up point, ψ is the amplitude of the disturbance which causes the stream to break up, and η is the viscosity of the fluid.

2.1.2. The shape of water streams in free fall

The shape of a fluid stream of circular cross-section, falling vertically under gravity, has been found by solving the Navier-Stokes equations in cylindrical coordinates.

$$\rho\left(u_r\frac{\partial u_z}{\partial r} + u_z\frac{\partial u_z}{\partial z}\right) = \rho g - \frac{\partial P}{\partial z}$$
$$\rho\left(u_r\frac{\partial u_r}{\partial r} + u_z\frac{\partial u_r}{\partial z}\right) = -\frac{\partial P}{\partial r} \qquad (2)$$

The z-axis is the axis of symmetry of the falling water stream, the r-axis is normal to z, ρ is the density of the fluid, u is the velocity of the fluid, P is the hydrostatic pressure in the fluid, and g is gravitational acceleration.

A number of approximations can be made to simplify these equations. For water streams, the viscosity of water has negligible effect, the radius of the stream is not a strong function of z, and the water velocity is a function of z only. The solution is then given by[7]

$$z = \frac{Q^2}{2\pi^2 g}\left(\frac{1}{R^4} - \frac{1}{R_0^4}\right) + \frac{\gamma}{\rho g}\left(\frac{1}{R} - \frac{1}{R_0}\right) \qquad (3)$$

where Q is the volume flux of fluid in m^3s^{-1}, R is the radius of the stream, R_0 is the radius of the nozzle, and γ is the surface tension of the fluid.

The predictions of this equation are compared to experimentally measured values for two relevant streams in figure 6. We can reasonably assume that streams issuing from small nozzles ($\leq$ 2.5 mm diameter) have a shape which is cylindrical rather than tapered.

2.2. Stream optics

Monochromatic excitation light was delivered to the base of the falling analyte stream through the centre fibre of an optical fibre bundle. We assume that the falling analyte stream is cylindrical in shape, and the optical fibre probe is centred on the axis of rotational symmetry of the cylinder, as shown in figure 2. The probe is considered to be a single, circular emission and collection aperture (ie, the emission and collection cones of the probe fibres completely overlap). This is valid for long lengths of analyte, in which the emission and collection cones will almost completely overlap, and the region in which there is little overlap between the cones is not affected by the presence of the capillary. The aperture is assumed to be smaller than the cylinder cross section, and to accept light over a smaller range of angles than that guided by the falling analyte stream. Emission from the analyte is assumed to be isotropic, which is valid in the small range of angles, 0 to ω_{input}, over which it is collected. Only light that is fully guided by the collection fibres is considered here, and some unguided, or leaky, optical fibre modes can propagate very efficiently over short lengths of fibre, so we expect to derive a slight underestimate of the total collected flux.

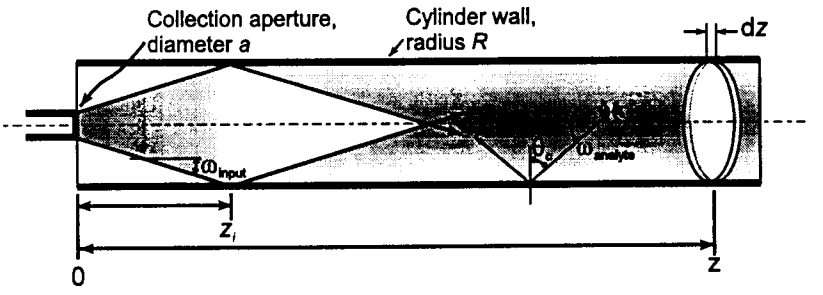

Figure 2 Coupling the optical fibre probe to the analyte stream. A differential element of collected flux $d\Phi$ is considered to originate from the differential slice of thickness dz.

Consider a cylinder of an aqueous analyte as an optical waveguide. Any light making an angle of less than $\omega_{analyte}$ to the axis will undergo repeated total internal reflection, where $\omega_{analyte}$ is equal to $90°-\theta_c$, and θ_c is the critical angle given by Snell's law. The numerical aperture *NA* of any optical element is defined in equation 4, where ω is the maximum ray angle accepted by the element, and n is the refractive index of the medium in which the ray is travelling. A cylinder of water surrounded by air has a *NA* of 0.88

$$NA = n\sin(\omega) \tag{4}$$

Excitation light diverges from the probe aperture until it intersects the cylinder wall, at the point marked z_i in figure 2. Because the cylinder *NA* is much larger than that of the fibre, all of this light is reflected back towards the centre of the cylinder. Fluorescent or Raman light is emitted within the cylinder, and some of this light will follow the reverse path back to the collection aperture.

The proportion S of the light emitted by the analyte that is guided towards one end of the cylinder is given by equation 5. For a cylinder of water, S is equal to 0.12.

$$S = \frac{2\pi(1-\cos(\omega_{analyte}))}{4\pi} = \sin^2\left(\frac{\omega_{analyte}}{2}\right) \tag{5}$$

However, it is impossible to make use of all of this light unless it is incident directly onto a detector (possibly via an optical filter). If we wish to transmit all of the light to more complex optical instrumentation then we require impractically fast collection optics; an *NA* of 0.88 corresponds to an f/# of 0.57. In this work, resolution requirements set by the spectrograph further limited the useful *NA* to 0.17. The most efficient means of coupling light to the spectrograph was to allow the analyte stream to fall directly onto the optical fibre probe.

For a collection aperture perfectly matched in size to the water cylinder cross section, the coupling efficiency L_{NA} between them is given by equation 6, where Ω_{input} is the solid angle over which light is collected by the probe, and $\Omega_{analyte}$ is the solid angle of the light guided by the cylinder.

$$L_{NA} = \frac{\Omega_{input}}{\Omega_{analyte}} = \frac{4\pi\sin^2(\omega_{input}/2)}{4\pi\sin^2(\omega_{analyte}/2)} \tag{6}$$

(Even by using input optics with f/# = 1 (NA of 0.5) we could only collect 30% of the light confined by the water cylinder, ie only 4% of the total emitted light.)

In the case where the cylinder is larger than the collection aperture, the coupling efficiency due to radius mismatch is given by equation 7[8].

$$L_{radii} = \frac{a^k}{R^k} \tag{7}$$

Here a is the radius of the aperture, R is the cylinder radius, and k is a constant between 1 and 2, which depends on the distribution of scattered light within the cylinder. A value of k=1 represents the case where all rays pass through the cylinder axis, whereas k=2 represents the case where skew rays carry an equal amount of energy (ie all waveguide modes are equally excited). In these experiments, the excitation light was delivered to the cylinder under the conditions for k=1, and if the cylinder wall was perfectly smooth we could expect the emitted light to have a similar distribution. However, we expect random perturbations of the falling stream wall to randomise the ray paths so that the irradiance distribution on any cross section is isotropic, and k=2.

The two equations 6 and 7 multiply to give the fraction of flux transferred from the falling analyte stream to the probe. To find the total flux collected, we introduce a differential flux element $d\Phi(z)$. This is the photon flux scattered *and then collected* from a cylindrical differential volume element (cross-section) of thickness dz, at a distance z from the probe, as shown in figure 2.

Before the emission and collection cone intersects the cylinder wall at z_i the cylinder has no effect on the amount of flux collected. Beyond the point z_i the average irradiance on a cylinder cross section must be constant, assuming that no light is absorbed. By reciprocity, the flux collected by the aperture must also be constant beyond this point, and in the absence of absorption $d\Phi(z)$ is constant too.

For the general case where the sample absorbs, $d\Phi(z)$ is a function of z, and is given by equation 8.

$$\begin{aligned} d\Phi(z) &= P_0 n_o \sigma \cdot \exp(-(\alpha_{ex}+\alpha_{em})z) \cdot S \cdot L_{NA} \cdot L_{radii} \cdot dz \\ &= P_0 n_o \sigma \exp(-(\alpha_{ex}+\alpha_{em})z) \cdot \sin^2(\omega_{input}/2) \cdot \frac{a^k}{R^k} \cdot dz \end{aligned} \tag{8}$$

Here P_0 is the total flux emitted from the probe tip, n_o is the number density of scattering molecules, and σ is the total scattering cross section in the direction of collection. The variables α_{ex} and α_{em} are the absorption coefficients at the excitation and emission wavelengths respectively. If α_{ex} and α_{em} are both small, then we can expect $d\Phi$ to be approximately constant. Equations 6-8 are only valid for the length of cylinder $z>z_i$; before this point the flux collected by the probe is unaffected by the presence of the cylinder.

By integrating the flux excited and then collected along a cylinder of length z_c, the expression for the total flux collected, Φ, is given by equation 9.

$$\begin{aligned} \Phi(z_c) &= \int_{z_i}^{z_c} d\Phi(z) \cdot dz + \Phi_{BP}(z_i) \\ &= \sin^2(\omega_{input}/2) \cdot \frac{a^k}{R^k} \cdot \frac{P_0 n_o \sigma}{\alpha_{ex}+\alpha_{em}} \left(\exp(-(\alpha_{ex}+\alpha_{em})z_c) - \exp(-(\alpha_{ex}+\alpha_{em})z_i)\right) + \Phi_{BP}(z_i) \end{aligned} \tag{9}$$

The constant $\Phi_{BP}(z_i)$ is the flux collected by a bare probe between z=0 and $z=z_i$. If the capillary is long (large z_c), or narrow (small z_i) $\Phi_{BP}(z_i)$ may be ignored. In this work we have presented our results in terms of the enhancement N, which is the ratio of the intensity measured by the probe coupled with the falling analyte stream $\Phi(z_c)$ to that measured using the probe alone $\Phi_{BP}(\infty)$. $N(z)$ shares the same dependance on the falling stream parameters as $\Phi(z)$.

From equation 9 we see that when $\Phi_{BP}(z_c)$ is negligible the flux collected from a falling analyte stream, and hence the enhancement N, is proportional to R^{-k}, where we expect k=2 due to perturbations of the cylinder wall.

3. EXPERIMENTAL METHODS AND RESULTS

Three experiments are described here. The first was to determine the maximum stable lengths which we could hope to produce, the second determined the shapes formed by the falling streams, and the third was a

measurement of the fluorescence collected from the falling analyte stream.

3.1. Stream stability experiments

To test the predictions of equation 1, a number of water streams were established, and their stability estimated using the apparatus shown in figure 3. The water pressure was maintained using a constant head device, into which water flowed from an elevated reservoir. In this way, the amplitude of vibrations caused by pressure fluctuations in the fluid was minimised. Light from an LED was coupled into the top of each stream using a lens. For each nozzle, the water flux was gradually increased, while the point of first break-up of the stream was estimated visually from the right-angle scattered light.

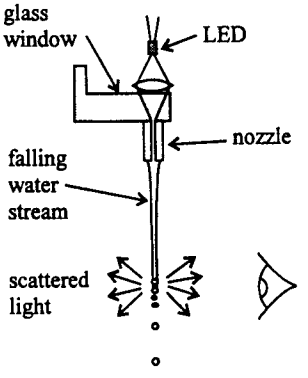

Figure 3. The apparatus used to determine the stable length of falling water streams.

Two extremes of behaviour were observed, believed to correspond to regions of laminar flow and turbulence, with a transition region in between. As the water velocity was increased, the stream's stable length increased, up to a point where the stream began to break up at much shorter lengths. Streams in the low velocity region were more stable than those in the high velocity region, with clearer break-up points. As we were interested in creating the longest stable streams, we concentrated on the low velocity region.

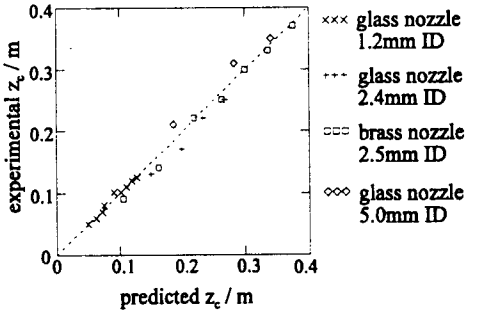

Figure 4. Predicted vs experimental values of the critical stream length, for a variety of nozzle sizes

Data from low velocity streams were fitted to equation 1 using the method of least squares, assuming that the same amplitude ψ would apply in each case, and varying the value of ψ to give the best fit. The critical stream radius, R_c, was calculated using equation 3. The agreement between experimental data and predicted values of the critical stream length is shown in figure 4. Slight systematic differences between the different nozzles could be explained by either different mechanical roughnesses, or slightly different nozzle weights, resulting in a different response to external vibrations. Both of these could have affected the amplitude of the initial disturbance (ψ).

3.2. Water stream shapes

The shapes of water streams exiting from the nozzles (diameters ≤ 7 mm) were determined for a range of flow rates.

The nozzles consisted of approximately 100 mm lengths of cylindrical glass capillary. These thin tubes were sufficiently long to ensure that the fluid exited the nozzle with laminar flow. The capillaries had been cleaved perpendicular to the axis to give a clean, sharp orifice edge. Water streams produced using a variety of nozzle sizes and flow rates were photographed, and measurements were taken from the images using calipers. The theory was shown to be valid over the entire range of diameters and flow rates of interest here, and results are displayed below for two different flow rates Q, and nozzle radii R_0.

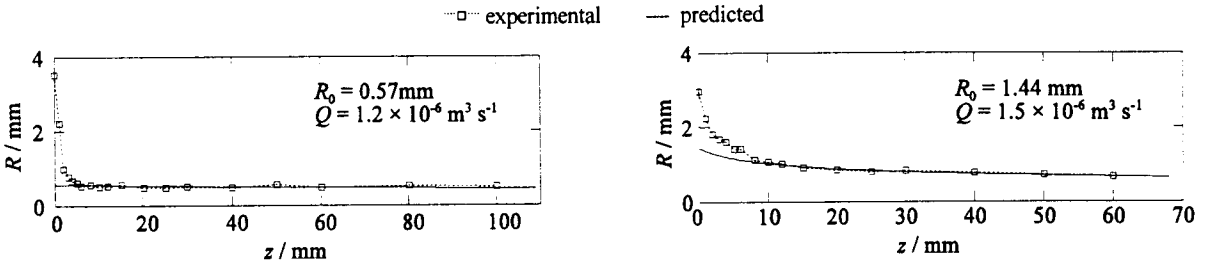

Figure 7 Predicted and experimental stream diameters, for two different sized nozzles.

At the top of each stream the water wetted the entire end of the capillary, which was considerably larger than the bore. Therefore, the streams were much wider at the top than equation 3 predicts, but the stream radius quickly approached the prediction. This behaviour is not believed to affect the stability of streams at large distances from the nozzle.

Identically shaped nozzles were constructed from different materials in order to test this hypothesis. Tubes of cleaved glass, machined brass and machined PTFE, with identical dimensions, were used to establish water streams under the same conditions. Up to approximately 50 g of Plasticine was attached to each nozzle to reduce the amplitude of vibrations, and to ensure that the nozzle masses were approximately the same in each case. The end of the glass nozzle was fully wetted, the brass nozzle end was partially wetted and the PTFE nozzle end was not wetted at all. Despite these variations, no significant difference between any of the streams could be found, in either their shape at large values of z, or their stability.

For the purpose of enhancing fluorescence collection, narrow streams were required, with nozzle bores of 1.0 - 2.5 mm, it was not practical to produce narrower bore streams. The assumption that the falling stream is cylindrical, rather than tapered, is most valid for the streams issuing from the smaller nozzles.

3.3. Fluorescence collection enhancement

3.3.1. Experimental

A schematic diagram of the equipment used in these experiments is given in figure 8. Light was delivered to, and collected from, a falling analyte stream via a multiple optical-fibre bundle (Oxford Electronics, UK). All of the fibres were identical, 95 μm core diameter, 105 μm outer diameter (including the polyimide buffer), step index fibres, with an *NA* of 0.22. The fibres were bonded into an SMA type ferrule, with the collection fibres arranged in 3 concentric rings around a single, centrally-located light-delivery fibre. The 6 fibres in the first ring were arranged on a radius of 128 μm, the 13 fibres in the second ring were on a radius of 240 μm, and the 19 fibres in the outer ring were on a radius of 336 μm. The approximately circular probe tip had a diameter of 0.8 mm. At the

other end of the probe cable, the collection fibres (all six fibres from the inner-most ring, 10 fibres from the middle ring, and 10 from the outer ring) were arranged to form a 3 mm vertical array, input to a grating/CCD spectrograph. The array height formed a good match to the height of the CCD detector array at the output focal plane of the spectrograph.

30 mW of light at 676 nm was emitted by a laser diode (CorkOpt PC-670-D), and filtered through two dielectric stack band-pass filters (CVI Corp. F10-676.4-4 and Infra-Red Engineering LDF-670). Light was coupled into the delivery fibre using anti-reflection coated aspherical lenses. 10.6 mW of light was delivered by the probe tip.

The spectrograph used to measure the fluorescence spectra comprised a concave holographic diffraction grating (Instruments SA, f/1.7, 400 lines/mm) and a cooled CCD detector (Hamamatsu C5809-0907). The light received via the 27 optical fibres was collimated, filtered through 9 mm of Schott RG-715 coloured glass and then refocused onto the spectrograph slit (100 μm wide and 3 mm tall). The CCD was controlled by a PC via a National Instruments Lab PC+ data acquisition card. The detector noise was shot noise limited.

Four falling analyte streams were studied, formed from 30 mm sections of blackened brass capillary tube of approximately 10 mm external diameter, and 1.0 mm, 1.5 mm, 2.0 mm, and 2.5 mm internal diameter. The holes were drilled on a lathe, and the nozzles blackened using a commercial brass blackening chemical. The nozzles were inserted 15 mm into the end of a 1.2 m long section of silicone rubber tubing, and held in place by friction. The silicone rubber tube was clamped approximately 10 mm above the nozzle in a vertical translation stage.

The analyte was pumped to a 200 mℓ header tank approximately 1 m above the nozzle by a peristaltic pump from a reservoir below the nozzle. The level of liquid in the header tank was held essentially constant, by means of an overflow pipe for excess fluid (K in figure 8). In this way, pressure fluctuations generated by the pump were minimised. The flow rate was controlled by the valve at the bottom of the header tank (marked L in figure 8). This was adjusted to give the longest stable stream possible, and then the flow rate was found by measuring the time taken by the stream to deliver 25 mℓ of the solution into a 30 mℓ beaker.

In each experiment, 1 ℓ of 12 μg/ℓ (±4%) fresh Panacryl Blue 5G (330%) (Holliday Dyes & Chemicals, UK) solution in de-ionised water was circulated around the flow rig. In order to establish the signal collected by the conventional fibre probe, a fluorescent measurement was taken with the bare probe dipped just below the surface of the reservoir before each measurement from the falling analyte stream. (The depth of analyte below the probe was approximately 90 mm for all four measurements. The measured intensity was not affected by the small variations of sample depth between each measurement.)

The optical fibre probe was mounted on an X-Y translation stage, positioned at the base of the falling stream of PB solution, and aligned at the centre of the falling stream. By adjusting the translation stage, the nozzle was butted against the probe tip to establish the position of z=0. The fluorescence collected by the optical fibres was recorded for increasing lengths of stream by retracting the nozzle and then realigning the probe.

The absorbance of Panacryl Blue at 60 mg/ℓ in deionised water was measured through a 10 mm path length cuvette, with a similar cuvette containing deionised water in the reference beam, using a Perkin-Elmer Lambda-9 spectrophotometer. In this way an accurate value of the absorbance of the 120 μg/ℓ solution could be calculated as at this weak concentration it was too low to measure directly with any accuracy. It was found that the absorption due to the dye was only significant at the excitation wavelenth, 676 nm. Over the spectrograph measurement wavelength range (710 nm to 860 nm) the solution absorbance was that of water. In this work the emission was measured at 740 nm, and the parameters α_{ex} and α_{em} were calculated as 1.40 m^{-1} and 2.39 m^{-1} respectively, using a literature value for the absorbance of water[9].

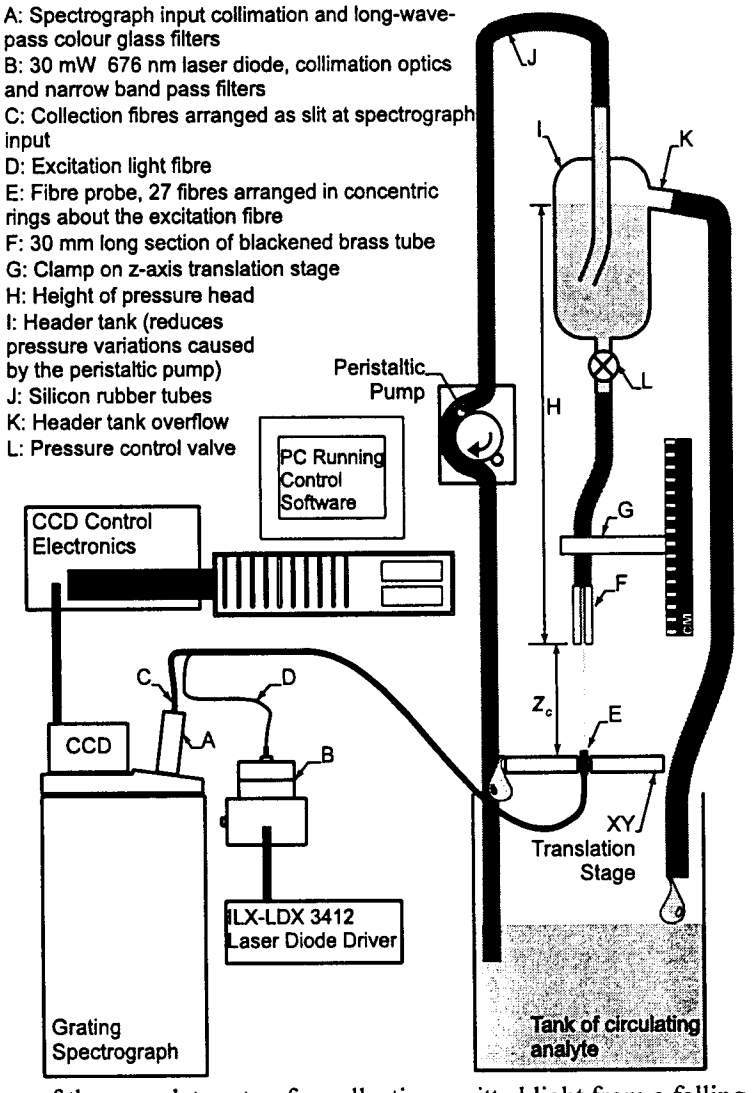

Figure 7 Schematic diagram of the complete setup for collecting emitted light from a falling analyte stream.

3.3.2. Fluorescence collection results and analysis

Due to environmental noise in the laboratory, and possibly pressure variations caused by the pump, the stable lengths of falling analyte were shorter than the maximum lengths found in our stability experiments. Breaks began to form in streams of length greater than approximately 80 mm, the exact point depending on which nozzle was used. These breaks caused brief reductions or loss of signal collected by the probe as they fell with the analyte. Beyond approximately 100 mm (160 mm for the 2.5 mm diameter nozzle) these breaks became so frequent that it was likely that the intensity of the recorded spectra would be reduced. Data from these unstable regions has not been presented here.

Fluorescence spectra were recorded over a 150 nm range for each jet length. In figure 9, a spectrum recorded with the bare probe is shown, superimposed on that from a 100 mm stream coupled with the probe. The slight distortion around the peak in the case of the 100 mm measurement is due to reabsorption of the fluorescent light by the solution during the longer path length back to the collection optics.

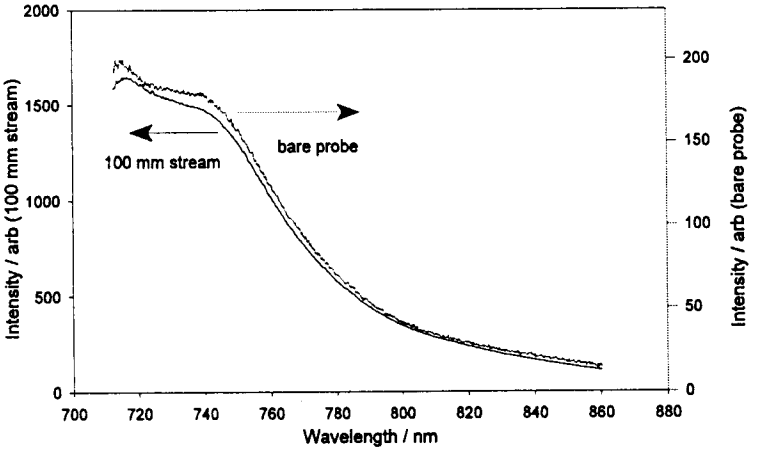

Figure 8 The fluorescence spectrum of Panacryl Blue 5G in water, measured with a bare fibre probe (upper trace; note the different axes), and with the same probe coupled with a 100 mm length falling analyte stream. The fluorescence was excited by 11 mW at 676 nm.

The variation of enhancement with stream length has been plotted against stream length in figure 10, for a number of different diameter nozzles. We have chosen to measure the enhancement at 740 nm as this wavelength is close to the emission maximum, and the solution absorbance is low. From the figure it is be seen that, for short stream lengths (less than 10 mm), the falling analyte stream made little difference to the amount of light collected by the fibre probe. The stream was very poorly defined in this region, illustrated in figure 11. With approximately 10 mm between the nozzle and the probe, the falling analyte stream formed a cylinder of liquid over the probe tip, and the enhancement began to rise in proportion to the length of the analyte stream.

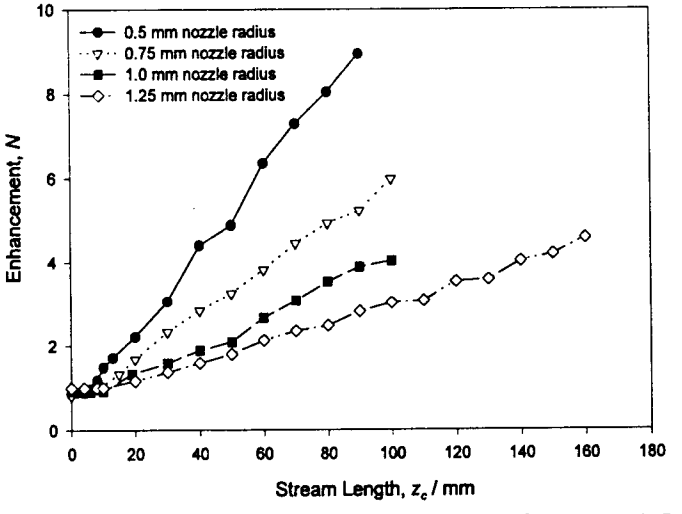

Figure 9 Enhancement factors vs stream lengths, for nozzle diameters of 1.0 mm, 1.5 mm, 2.0 mm and 2.5 mm.

The main contribution to the noise in these measurements is from the error in the position of the fibre probe in the X-Y plane. We expected to see a slight deviation from a straight line in these results due to sample absorbance, however no such deviation is apparent. We believe this is due to the tapered shape of the falling stream, which has the effect that $d\Phi(0)$ is greater for longer streams. We hope to account for this effect in future work.

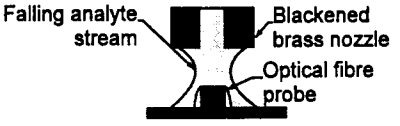

Figure 10 At stream lengths below 10 mm the falling stream is very poorly defined.

The flow rate, the radius of the falling stream at z=60 mm (calculated from equation 3), and the gradient of the enhancement dN(60) (ie dN/dz at z=60 mm, estimated from figure 10) for the streams are tabulated below. The probe radius a was 0.775 mm in each case. Equation 8 suggests that dN(60)·R_{60}^2 should be constant, which is seen to be the case.

Nozzle radius / mm	Flow rate, Q / 10^{-6}m^{3}s	Stream radius R_{60}/mm	Gradient of enhancement,dN(60) / mm	(dN(60)·R_{60}) / 10^{-3}mm^2	(dN(60)·R_{60}^2) / 10^{-3}mm^3
0.5	1.727	0.475	0.12±0.02	57±10	27±4.5
0.75	2.269	0.659	0.06±0.01	40±7	26.±4.3
1.0	3.181	0.825	0.05±0.015	41±10	34±10
1.25	4.039	0.974	0.025±0.01	24±10	24±9.6

4. CONCLUSIONS

We have modelled and demonstrated a novel means of enhancing the amount of light collected from a fluorescent emission measurement. The falling analyte stream (FAST) technique is equally suited to measurement of Raman light emission, and as we have shown, it is convenient to couple the falling analyte stream to an optical fibre probe. We have measured a maximum signal enhancement of 9 times in this work, but we so no reason why further enhancement to the apparatus, such as better vibration isolation, should not increase this value by a further factor of two.

Coupling excitation light in and out of the falling analyte stream from the top of the stream (similar to the arrangement illustrated as in figure 3) is possible, and would minimise the effect of random breaks in the stream (which would then occur further from the probe). In this way, noise in the measurements due to random break-up of the stream would be reduced.

ACKNOWLEDGMENTS

This work was supported by North West Water Ltd, UK, and the EPSRC, UK.

REFERENCES

1. Walrafen G E and Stone J, "Intensification of Spontaneous Raman Spectra by use of Liquid Core Optical Fibres", Applied Spectroscopy, **26**, pp. 585-589, 1972.

2. "Teflon AF Amorphous Fluoropolymer. A New Generation of Teflon Fluorocarbon Resins for High Performance", product information available from Du Pont (Wilmington, DE).

3. Mackenzie S J, Johnson M J, and Dakin J P, "Novel Configuration for Convenient and Sensitive Fluorescence and Raman Measurements of Liquids Over Optical Fibres", Proceedings of EnviroSense '97, Munich, 1997.

4. Strutt J W, Baron Rayleigh, "The Theory of Sound", Dover Publications, New York, 1945.

5. Goedde E F and Yuen M C, "Experiments on liquid jet instability", Journal of Fluid Mechanics, **40**, pp. 495-511, 1970.

6. Weber C, "Zum Zerfall eines Flüssigkeitsstrahles", Zeitschrift für Angewandte Mathematik und Mechanik, **2**, pp. 136-154, 1931.

7. Anno J N, "The mechanics of liquid jets", DC Heath, ISBN 0-669-00940-7, 1977.

8. Senior J M, *Optical Fibre Communications Principles and Practice Second Edition*, p. 222, Prentice Hall International (UK), Hemel Hempstead, UK, 1992.

9. Smith R C and Baker K S, "Optical properties of the clearest natural waters (200-800 nm)" Applied Optics, **20**, pp. 177-184, 1981.